J Solid State Electrochem (2017) 21:1365–1372
DOI 10.1007/s10008-016-3499-6

ORIGINAL PAPER

Kinetics of Li-ion transfer reaction at $LiMn_2O_4$, $LiCoO_2$, and $LiFePO_4$ cathodes

Agnieszka Swiderska-Mocek[1] · **Andrzej Lewandowski**[1]

Received: 9 November 2016 / Revised: 21 December 2016 / Accepted: 26 December 2016 / Published online: 7 January 2017

Abstract Kinetics of $LiFePO_4$, $LiMn_2O_4$, and $LiCoO_2$ cathodes operating in 1 M $LIPF_6$ solution in a mixture of ethylene carbonate and dimethyl carbonate was deduced from impedance spectra taken at different temperatures. The most striking difference of electrochemical impedance spectroscopy (EIS) curves is the impedance magnitude: tens of ohms in the case of $LiFePO_4$, hundreds of ohms for $LiMn_2O_4$, and thousands of ohms for $LiCoO_2$. Charge transfer resistances (R_{ct}) for lithiation/delitiation processes estimated from the deconvolution procedure were 6.0 Ω ($LiFePO_4$), 55.4 Ω ($LiCoO_2$), and 88.5 Ω ($LiMn_2O_4$), respectively. Exchange current density for all the three tested cathodes was found to be comparable ($0.55–1{\cdot}10^{-2}$ $mAcm^{-2}$, $T = 298$ K). Corresponding activation energies for the charge transfer process, $E_{ct}^{\#}$, differed considerably: 66.3, 48.9, and 17.0 $kJmol^{-1}$ for $LiMn_2O_4$, $LiCoO_2$, and $LiFePO_4$, respectively. Consequently, temperature variation may have a substantial influence on exchange current densities (j_o) in the case of $LiMn_2O_4$ and $LiCoO_2$ cathodes.

Keywords $LiMn_2O_4$ · $LiCoO_2$ · $LiFePO_4$ cathodes · Graphite anode · Impedance · Kinetic parameters · Lithium-ion battery

Introduction

Rechargeable Li-ion batteries have become major power sources in a growing number of applications, including the automotive industry. This creates new requirements such as high rate performance during both charging and discharging. To describe the rate limiting process, all internal system resistances must be known. Among several processes taking place in Li-ion batteries, the Li^+ charge transfer reaction at both the cathode and anode seems to be essential to gain insight into the internal cell impedance. The most studied anode materials are different carbons and $LiMn_2O_4$, while $LiCoO_2$ and $LiFePO_4$ are basic cathode materials. Kinetics of anodic [1–8] and cathodic processes [9–24] have been studied. Results of reported studies are not comparable. However, one of the most important factors is the resistance (impedance) associated with the charge transfer process, which has not been fully clarified for cathodes. The general aim of this study was to compare the charge transfer process taking place at $LiMn_2O_4$, $LiCoO_2$, and $LiFePO_4$ cathodes using the same methodology and electrolytes.

Experimental

Materials

$LiFePO_4$ (carbon coated, battery grade, Aldrich), $LiMn_2O_4$ (Aldrich), $LiCoO_2$ (Aldrich), carbon black (CB, Fluka), poly(vinylidene fluoride) (PVdF, M_W = 180,000 Fluka), lithium foil (Aldrich, 0.75 mm thick), and *N*-methyl-2-pyrrolidinone (NMP, Fluka) were used as received. $LiPF_6$ solution (1 M) in a mixture of ethylene carbonate and dimethyl carbonate (EC + DMC 1:1, Aldrich) was used as electrolyte.

Tested cathodes were prepared on golden current collectors by a casting technique from a slurry of electrode material, carbon black, and PVdF suspension in NMP. After solvent (NMP) evaporation at 120 °C in a vacuum, a layer of the electrode, containing the active material, the electronic conductor (CB), and a binder (PVdF) was formed.

✉ Agnieszka Swiderska-Mocek
agnieszka.swiderska-mocek@put.poznan.pl

[1] Faculty of Chemical Technology, Poznan University of Technology, 60 965 Poznan, Poland

Table 1 Parameters of tested electrodes (expressed versus mass of active material): mass m, specific BET surface area S_{BET}, real surface area S calculated as $m \cdot S_{BET}$, passivation film resistance R_f, resistance of charge transfer process R_{ct}, exchange current density j_o, activation energy of Li^+ transport in passivation film ($E_f^{\#}$), and of charge transfer process ($E_{ct}^{\#}$)

		$LiMn_2O_4$	$LiCoO_2$	$LiFePO_4$	CF_x [25]	G
Measured parameters						
m	mg	2.30 ± 0.01	2.40 ± 0.01	2.75 ± 0.01	–	4.00 + 0.01
S_{BET}	$m^2\ g^{-1}$	2.30 ± 0.048	2.05 ± 0.089	15.4 ± 0.061	93.6 ± 0.092	6.0 ± 0.068
R_f	Ω	102 ± 4.9	645 ± 17.2	4.9 ± 0.1	–	4.3 ± 0.3
R_{ct}	Ω	88.5 ± 4.2	55.4 ± 2.1	6.0 ± 0.1	–	13.9 ± 0.5
$E_f^{\#}$	kJ mol^{-1}	67.0 (r^2 = 0.948)	53.6 (r^2 = 0.985)	29.5 (r^2 = 0.982)	–	–
$E_{ct}^{\#}$	kJ mol^{-1}	66.3 (r^2 = 0.947)	48.9 (r^2 = 0.988)	17.0 (r^2 = 0.981)	–	[3, 5, 32]
Calculated parameters						
S	cm^2	52.9	49.2	423.5	–	240.0
$S \cdot R_{ct}$	Ωcm^2	$4.68 \cdot 10^3$	$2.73 \cdot 10^3$	$2.54 \cdot 10^3$	–	$3.34 \cdot 10^3$
j_o	$mAcm^{-2}$	$0.55 \cdot 10^{-2}$	$0.94 \cdot 10^{-2}$	$1.01 \cdot 10^{-2}$	$1.12 \cdot 10^{-4}$	$0.77 \cdot 10^{-2}$

Procedures and measurements

Electrochemical properties of the cells were characterized using electrochemical impedance spectroscopy (EIS) and galvanostatic charging/discharging tests. The cycling measurements were taken with the use of the ATLAS 0461 MBI multichannel electrochemical system (Atlas-Sollich, Poland). Impedance spectroscopy measurements were performed using the Gamry 1000 multichannel electrochemical system (USA) at different temperatures. Tested anodes were separated from metal-lithium counter and reference electrode by the glass microfiber GF/A separator (Whatmann, 0.4–0.6-mm thick), all placed in an adopted Swagelok® connecting tube. Typically, the mass of the lithium was ca. 31 mg (0.785 cm^2), while that of cathodes was 3.0–4.0 mg. The cells were assembled in a glove box in the dry argon atmosphere. After electrochemical measurements, the cells were disassembled and the cathodes were washed with DMC and dried in vacuum at room temperature. The morphology of electrodes was observed with a scanning electron microscope (SEM, Tescan Vega 5153). The BET surface of pristine electrode materials was determined with an Autosorb iQ apparatus (Quantochrome Instruments, UK) and particle size distribution with a Zetasizer Nano ZS (Malvern Instruments Ltd., UK).

Results and discussion

BET surface, size distribution, and SEM images

Specific surface area of cathode materials from BET analysis was between 15.4 and 2.05 $m^2\ g^{-1}$ (Table 1). Particle size distribution is shown in Fig. 1. $LiFePO_4$ and $LiCoO_2$

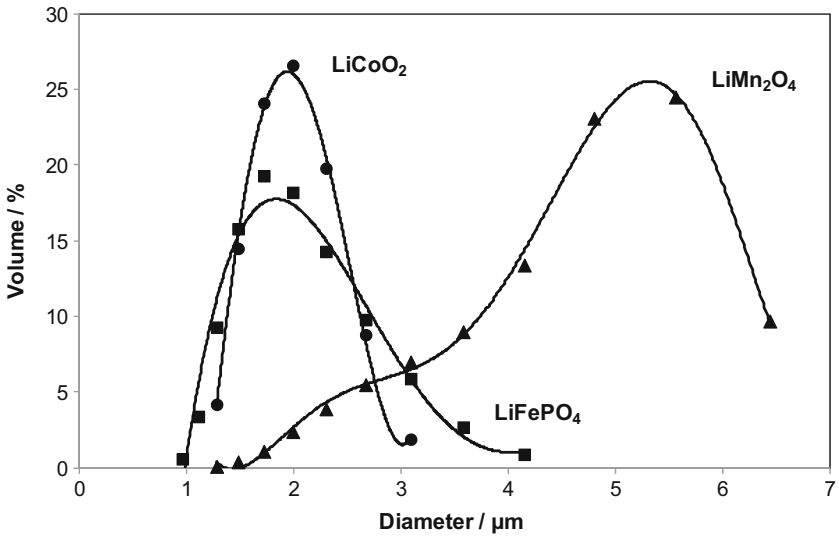

Fig. 1 Particle size distribution of electrode materials

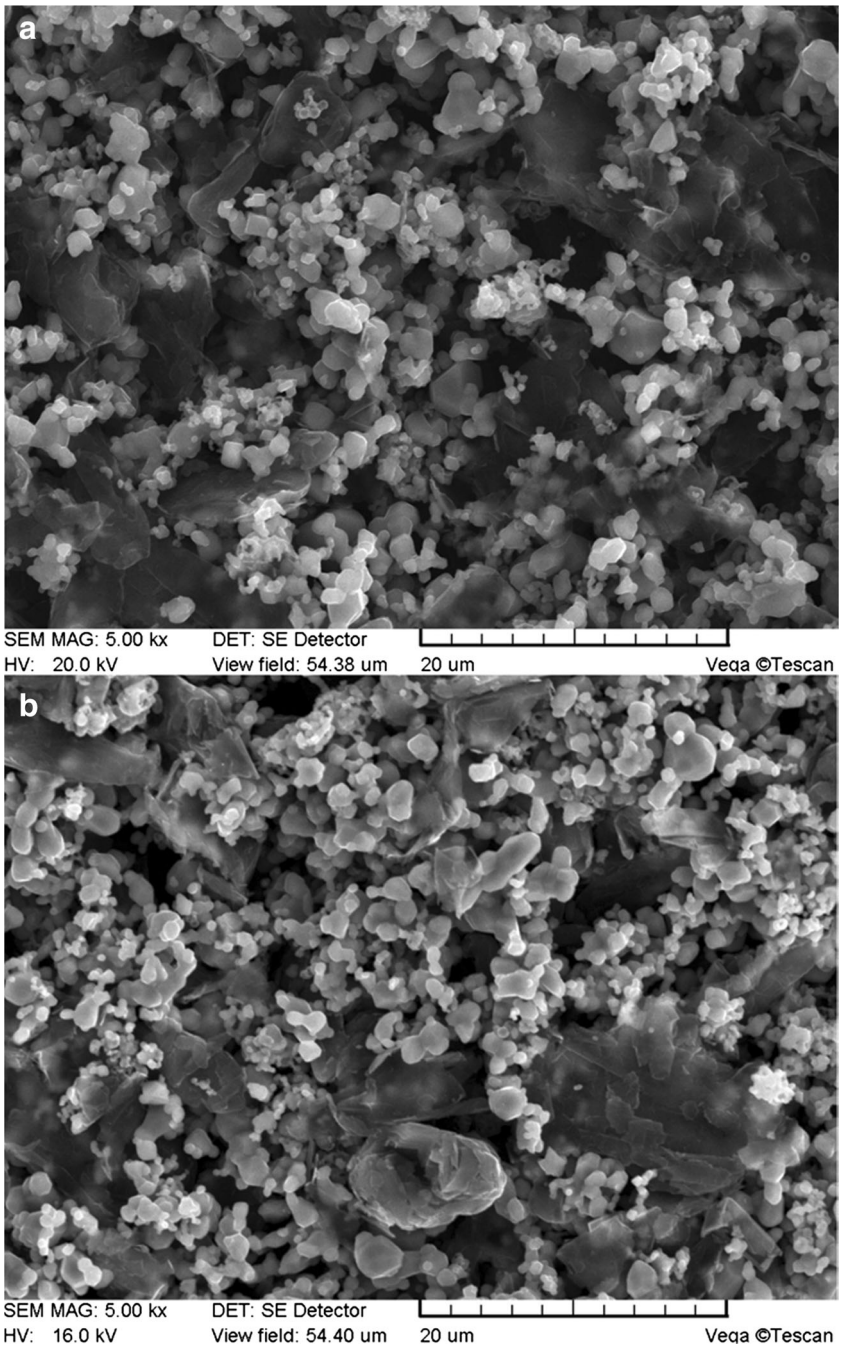

Fig. 2 SEM images of $LiMn_2O_4$ cathode **a** before and **b** after 4 cycles (magnification ×5000)

materials contained particles of diameters between 1 and 4 μm, with the maximum amount of ca. 2 μm. The size distribution of $LiMn_2O_4$ particles was broader (2 and 7 μm with a maximum at 4–6 μm). Figures 2, 3, and 4 show SEM images of cathodes (1) after electrode formation but before its cycling and (2) in the discharged state after the second cycle. In the case of all cathodes, their cycling results in the formation of small particles. In the case of $LiFePO_4$ and $LiMn_2O_4$, the diameter of particles remained similar while $LiCoO_2$ was converted into material of a smaller diameter.

Impedance and kinetic parameters

Figure 5 shows impedance spectra of tested cathode materials at room temperature. All curves consist of two semicircles at the high frequency region and a straight line at low frequencies (in the case of $LiFePO_4$, only a part of the first semicircle can be seen). The most striking difference is the impedance (resistance) magnitude: tens of ohm in the case of $LiFePO_4$, hundreds of ohm for $LiMn_2O_4$, and thousands of ohm for $LiCoO_2$. Impedance spectra were deconvoluted according to the equivalent circuit shown in Fig. 6. It was selected from a

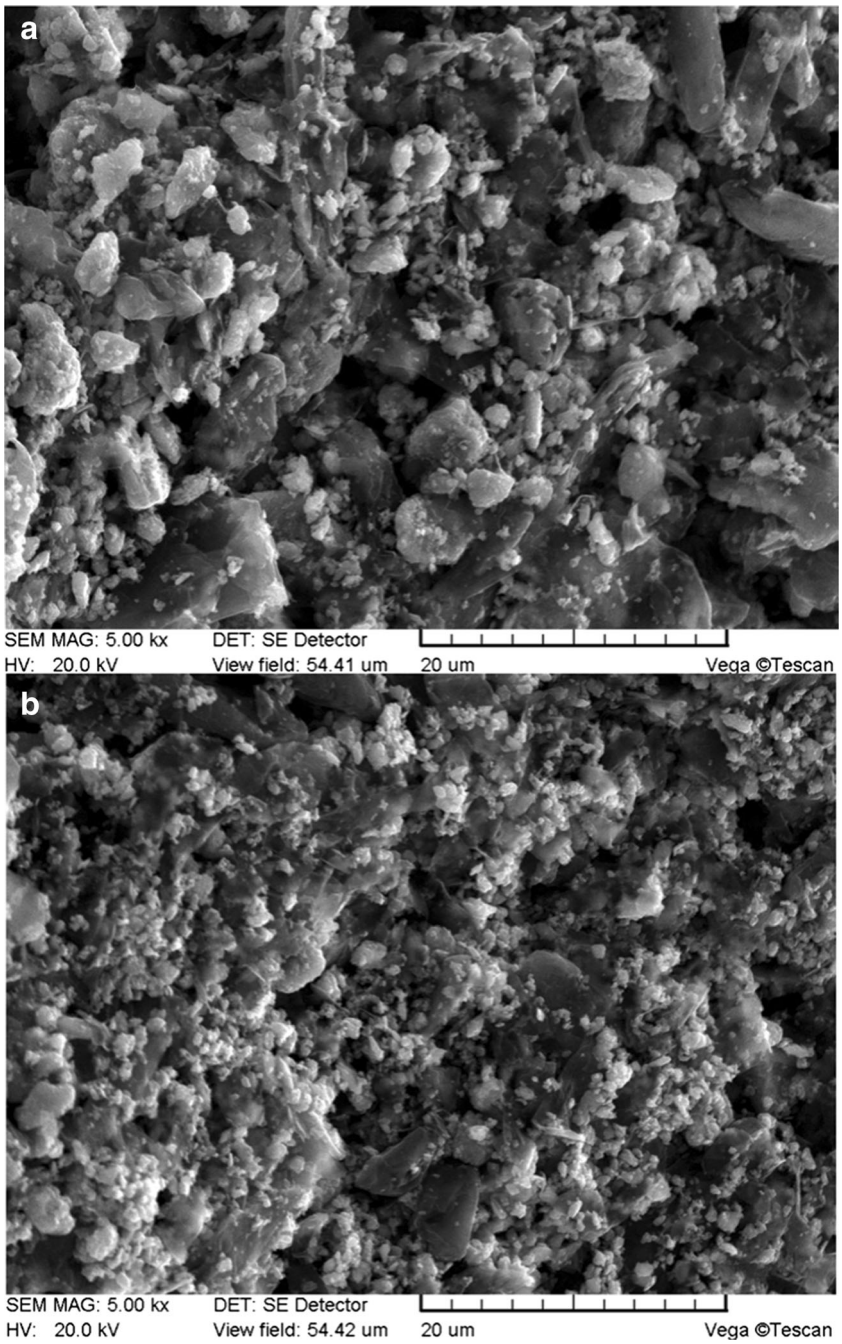

Fig. 3 SEM images of $LiCoO_2$ cathode **a** before and **b** after 4 cycles (magnification ×5000)

library of circuits based on two time constants due to best correlation of fits with experimental data. Passivation film (R_f) and charge transfer (R_{ct}) resistances obtained from the deconvolution procedure are shown in Table 1. Both R_f and R_{ct} given in ohms are expressed versus the geometrical surface area of electrodes (1.27 cm^2). It can be seen from Table 1 that resistance of the passivation film differs by two orders of magnitude depending on the electrode material: it was 4.9 Ω for $LiFePO_4$, ca. 20 times more for $LiMn_2O_4$ (102 Ω), and as high as 645 Ω for $LiCoO_2$. Charge transfer resistances (R_{ct}) estimated from the deconvolution procedure were between 6.0 and 88.5 Ω (Table 1). Those resistances can be expressed against the anode real surface area A (estimated from BET measurements $S = m \cdot S_{BET}$) as $R_{ct} \cdot S$ (expressed in Ωcm^2).

Charge transfer resistances may be converted into surface area independent of exchange current densities:

$$j_0 = \frac{RT}{FS}\frac{1}{R_{ct}} \tag{1}$$

Both $R_{ct} \cdot S$ and j_o values are given in Table 1. It can be seen that while charge transfer resistances differ for one order of

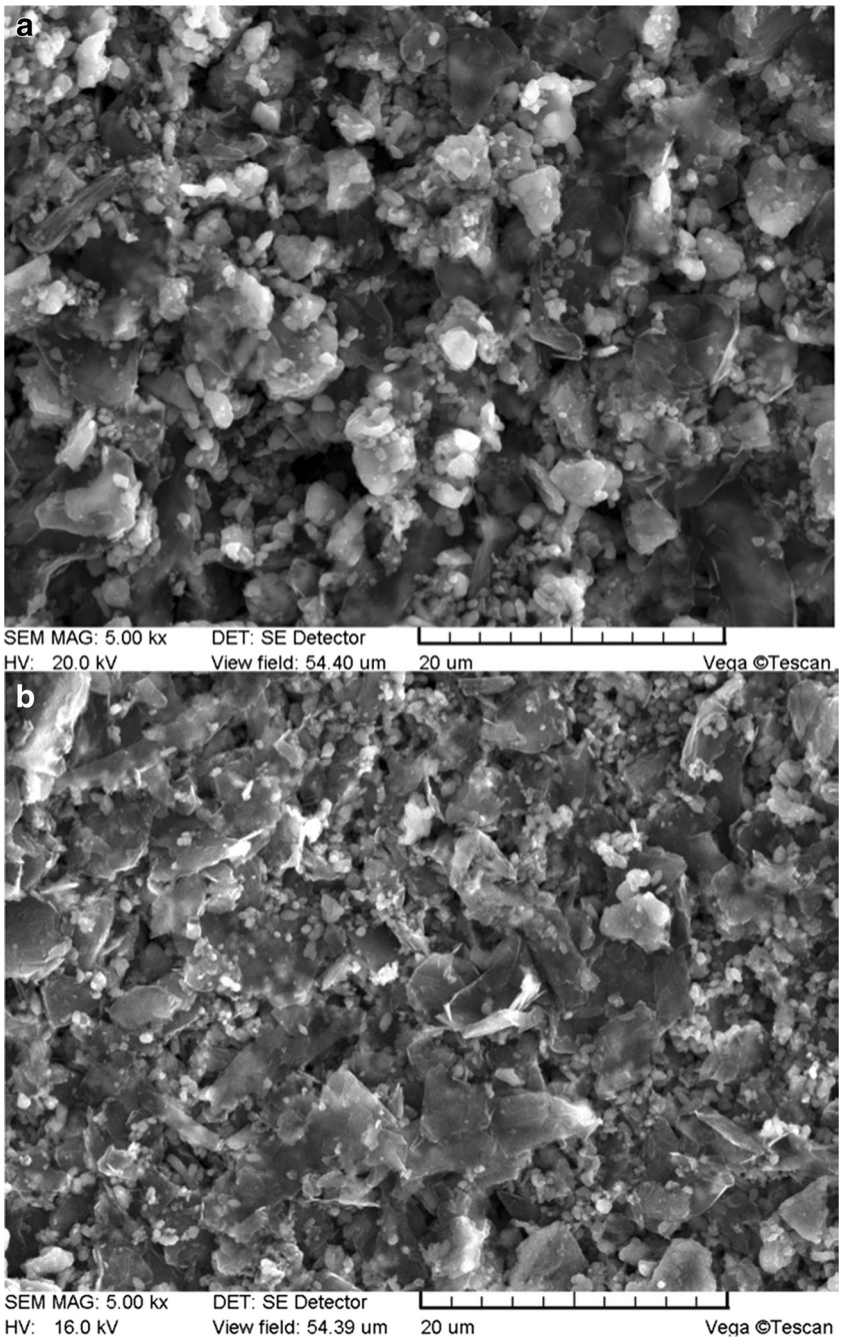

Fig. 4 SEM images of $LiFePO_4$ cathode **a** before and **b** after 4 cycles (magnification ×5000)

magnitude, the corresponding $R_{ct} \cdot S$ values are comparable: from ca. 4.7 to ca. 2.5 kΩcm^2. Consequently, exchange current density for all the three cathode materials is also comparable, amounting to 10^{-2} mAcm^{-2}: from ca. 0.55 10^{-2} mAcm^{-2} ($LiMn_2O_4$) to ca. $0.94 \cdot 10^{-2}$–1.01 10^{-2} mAcm^{-2} ($LiCoO_2$ and $LiFePO_4$). Exchange current densities can be found in the literature for the $LiFePO_4$ material [16–18]. In general, j_o values are reported in a broad range between 10^{-5} mAcm^{-2} (5.19 10^{-5} mAcm^{-2} [17], 2.12 10^{-5} mAcm^{-2} [18]), and 10^{-1} mAcm^{-2} ($1.7 \cdot 10^{-1}$ mAcm^{-2} [16]). However, a comparison of the present results with literature data is difficult because (i) different solvents or electrolytes were used and (ii) the real surface areas of electrodes were not reported or even not taken into account in calculations. For the other cathodes ($LiCoO_2$ and $LiMn_2O_4$), $R_{ct} \cdot S$ and j_o values are not available.

Kinetic parameters of cathodes may be compared to the corresponding data for the metallic lithium [9, 25–30] anode. A typical reported value is of the order of 10–10^{-1} mA cm^{-2}, depending on the solvent, electrolyte, and its concentration [30]. Exchange current density values, expressed versus the active material specific surface, suggest that the kinetics of the charge transfer taking place at the cathode is slower in

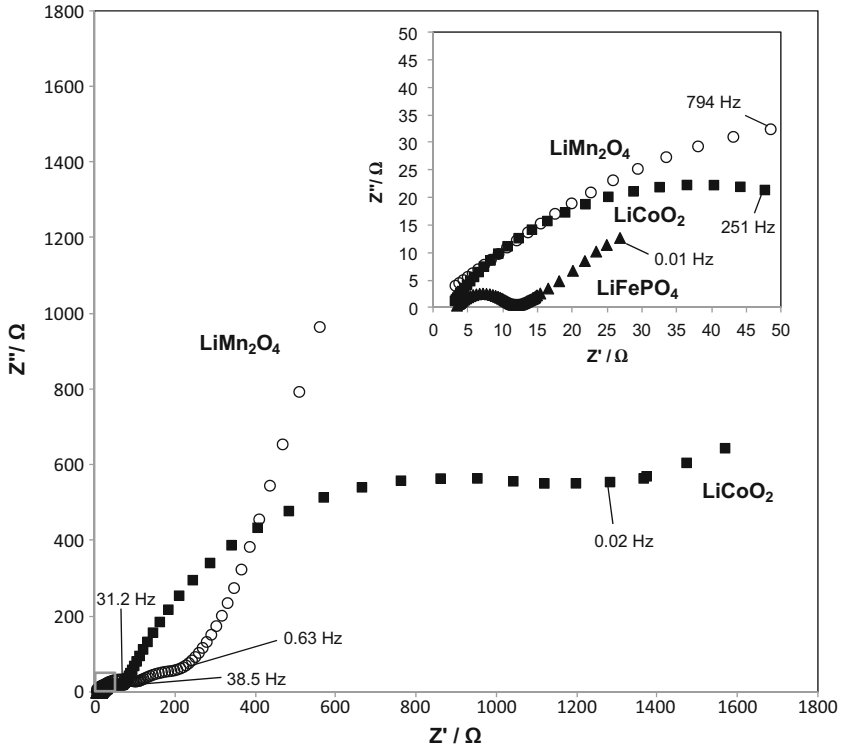

Fig. 5 Impedance spectra of $LiMn_2O_4$, $LiCoO_2$, and $LiFePO_4$ cathodes taken at 298 K. Counter-electrode: lithium metal

comparison to metallic lithium, while the surface area is larger. To our knowledge, available literature does not present exchange current densities for LiC_6 (graphite) anodes working together with classical $LiPF_6$ electrolytes. Generally, R_{ct} values determined from impedance spectroscopy for a lithiated graphite anode can be found in the literature; however, resistance depends on the electrode size (real surface area), which usually is not mentioned. Therefore, the j_o value for LiC_6 was measured in the present study in the same way as for cathodes (the impedance spectrum for the LiC_6 anode is shown in Fig. 7) and data are listed in Table 1. It can be seen that the exchange current density is comparable to that characteristic of anodes ($0.77 \cdot 10^{-2}$ mA cm^{-2}).

Values of R_f and R_{ct} measured at different temperatures and plotted as $-\ln R = f(T^{-1})$ provide electrode size-independent charge transfer activation energy $E^{\#}$. Figure 8 shows the Arrhenius plot for a $LiFePO_4$ cathode as an example. Both $E_f^{\#}$ and $E_{ct}^{\#}$ values for all cathodes are shown in Table 1. It can be seen that activation energies for the Li^+ ion conduction in passivation film and charge transfer reaction are similar in the case of $LiMn_2O_4$ and $LiCoO_2$ while in the case of the $LiFePO_4$ cathode, both $E_f^{\#}$ and $E_{ct}^{\#}$ are considerably lower. Activation energies for the charge transfer process taking places at cathodes can be found in the literature [11–15]. Again, a comparison of data is difficult due to different solvents, electrolytes, and their concentrations. Some data are reported for polymer electrolytes. In addition, the state of cathodes intercalation is different, which is equivalent to a

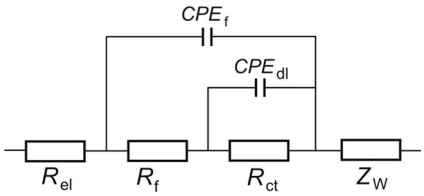

Fig. 6 Equivalent circuit used for impedance spectra deconvolution

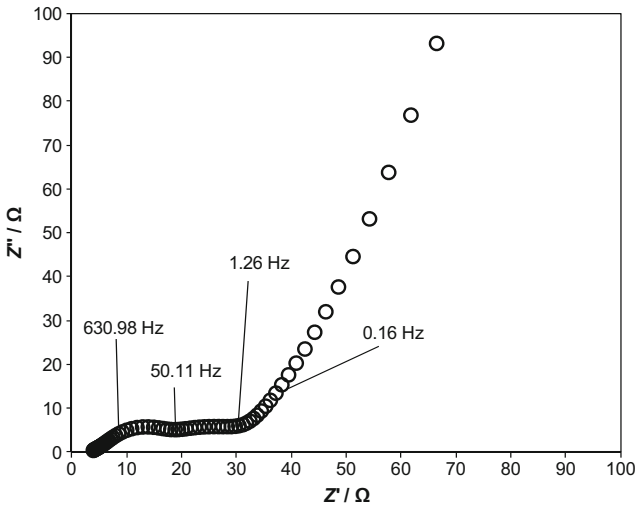

Fig. 7 Impedance spectrum of LiC_6 anode taken at 298 K. Counter-electrode: lithium metal

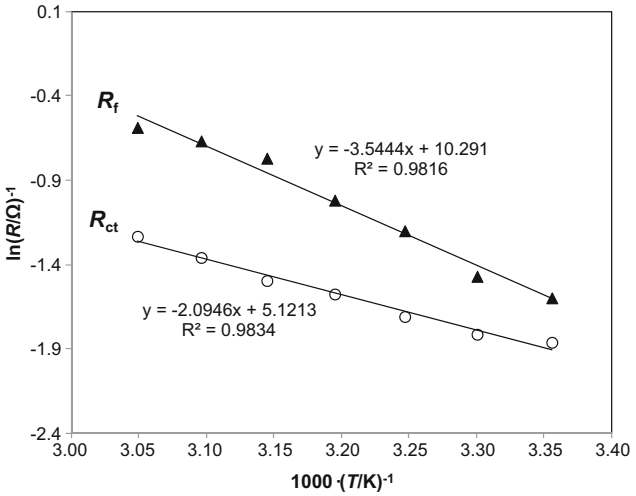

Fig. 8 Arrhenius plot for the charge transfer (R_{ct}) and passivation film (R_f) resistances for the $LiFePO_4$ electrode

comparison of different compounds. For example, the $E_{ct}^{\#}$ value found here for the $LiCoO_2$/1 M $LiPF_6$ in EC + DMC system is 48.9 kJmol^{-1}, comparable to that reported for the $LiCoO_2$/1 M $LiClO_4$ or $LiCF_3SO_3$ in PC (46–48 kJmol^{-1} [14]). Both values were measured at a potential of ca. 3.9 V versus metallic lithium. The corresponding activation energy measured at a higher potential (4.2 V), equivalent to a lower degree of intercalation, was reported to be much lower (ca. 25 kJmol^{-1} [15]).

Compatibility of cathodes with the LiC_6 anode

Li-ion batteries typically contain a carbon anode, which capacity (for graphite ca. 370 mAh g^{-1}) is usually higher in comparison to that characteristic of cathodes (Table 2). However, the capacity of the CF_x material is very high (ca. 900 mAh g^{-1}), and hence, literature kinetic data for this cathode [31] are also shown in Table 2. The ratio of the cathode and graphite mass should be equal to the corresponding ratio of specific capacity ($n_c/n_G = q_c/q_G$) to maximize active material utilization. The ratio m_c/m_G indicates also the mass of the cathode compatible with 1 g of carbon material. It can be seen from Table 2 that the mass ratio n_c/n_G for $LiMn_2O_4$, $LiCoO_2$, and $LiFePO_4$ cathodes is between 3.08 and 2.18 in contrast to the CF_x material ($n_{CFx}/n_G = 0.41$). On the other hand, from the point of view of power, the ratio of anodic and cathodic charge transfer resistance should be close to 1 (a more resistive electrode determines the operation rate). The ratio of cathodic and anodic resistances R_c/R_G can be calculated from the ratio of electrode surface S_G/S_c and exchange current densities j_o^G/j_o^c:

$$\frac{R_c}{R_G} = \frac{S_G j_o^G}{S_c j_o^c} \tag{2}$$

The R_c/R_G ratio values shown in Table 2 fall within a broad range between 0.13 and 10.04. While $LiMn_2O_4$ and $LiCoO_2$ cathodes ($R_c/R_G \approx 1$) are kinetically compatible with the carbon anode, the situation in the case of other cathodes is different. The $LiFePO_4$ material shows resistance by one order of magnitude lower than the equivalent amount of carbon. In contrast, the CF_x cathode is characterized by resistance by one order of magnitude higher than the equivalent amount of the anode.

Conclusions

The most striking difference of EIS curves is the impedance magnitude: tens of ohms in the case of $LiFePO_4$, hundreds of ohms for $LiMn_2O_4$, and thousands of ohms for $LiCoO_2$. Charge transfer resistances (R_{ct}) for the lithiation/delitiation process estimated from the deconvolution procedure were 6.0 Ω ($LiFePO_4$), 55.4 Ω ($LiCoO_2$), and 88.5 Ω ($LiMn_2O_4$). Exchange current density for all the three tested cathodes was found to be comparable ($0.55\cdot10^{-2}$–$1\cdot10^{-2}$ mAcm^{-2}, T = 298 K).

Corresponding activation energies for the charge transfer process, $E_{ct}^{\#}$, differed considerably: 66.3, 48.9, and 17.0 kJmol^{-1} for $LiMn_2O_4$, $LiCoO_2$, and $LiFePO_4$,

Table 2 Calculated compatibility parameters of graphite anode (G) and cathodes (c): theoretical capacity q, mass n of cathode material compatible with 1 g of graphite (n_c = 1 g·(q_G/q_c)), real surface area of electrode material S (calculated as $n\cdot S_{BET}$), ratio of graphite and cathode real surface (S_G/S_c), exchange current density (j_o^G/j_o^c), and charge transfer resistance (R_c/R_G)

		$LiMn_2O_4$	$LiCoO_2$	$LiFePO_4$	CF_x [25]	G
q	mAh·g^{-1}	120	140	170	900	370
n	g	3.08	2.64	2.18	0.41	1.00
S	cm^2	$7.08\cdot10^4$	$5.41\cdot10^4$	$3.36\cdot10^5$	$3.84\cdot10^5$	$6.00\cdot10^4$
S_G/S_c		0.85	1.11	0.18	0.16	–
j_o^G/j_o^c		1.31	0.77	0.71	64.29	–
R_c/R_G		1.11	0.85	0.13	10.04	–

respectively. Consequently, temperature variation may have a substantial effect on j_o in the case of $LiMn_2O_4$ and $LiCoO_2$ cathodes.

Acknowledgements Support of grant NCN UMO/2013/09/B/ST4/00107 is gratefully acknowledged.

References

1. Abe T, Fukuda H, Iriyama Y, Ogumi Z (2004) Solvated Li-ion transfer at interface between graphite and electrolyte. J Electrochem Soc 151:A1120–A1123
2. Xu K, Lam Y, Zhang SS, Jow TR, Curtis TB (2007) Solvation sheath of Li^+ in nonaqueous electrolytes and its implication of graphite/electrolyte interface chemistry. J Phys Chem C 111: 7411–7421
3. Yamada Y, Iriyama Y, Abe T, Ogumi Z (2009) Kinetics of lithium ion transfer at the interface between graphite and liquid electrolytes: effects of solvent and surface film. Langmuir 25:12766–12770
4. Wibowo R, Jones SEW, Compton RG (2010) Investigating the electrode kinetics of the Li/Li^+ couple in a wide range of room temperature ionic liquids at 298 K. J Chem Eng Data 55:1374–1376
5. Xu K, von Cresce A, Lee U (2010) Differentiating contributions to "ion transfer" barrier from interphasial resistance and Li^+ desolvation at electrolyte/graphite interface. Langmuir 26:11538–11543
6. Jow TR, Allen JL, Marx M, Nechev K, Deveney B, Rickman S (2010) Electrolytes, SEI and charge discharge kinetics of Li-ion batteries. ECS Trans 25:3–12
7. Yamada Y, Iriyama Y, Abe T, Ogumi Z (2010) Kinetics of electrochemical insertion and extraction of lithium ion at SiO. J Electrochem Soc 157:A26–A30
8. Lewandowski A, Biegun M, Galinski M, Swiderska-Mocek A (2013) Kinetic analysis of $Li|Li^+$ interphase in an ionic liquid electrolyte. J Appl Electrochem 43:367–374
9. Zeng X, Xu GL, Li Y, Luo X, Maglia F, Bauer C, Lux SF, Paschos O, Kim SJ, Lamp P, Lu J, Amine K, Chen Z (2016) Kinetic study of parasitic reactions in Lithium-ion batteries: a case study on $LiNi_{0.6}Mn_{0.2}Co_{0.2}O_2$. ACS Appl Mater Interfaces 8:3446–3451
10. Kim J, Kim M, Noh S, Lee G, Shin D (2016) Enhanced electrochemical performance of surface modified $LiCoO_2$ for all solid state lithium batteries. Ceramics Int 42:2140–2146
11. Li J, Yuan CF, Guo ZH, Zhang ZA, Lai YQ, Liu J (2012) Limiting factors for low-temperature performance in $LiFePO_4$/Li and graphite/Li half cells. Electrochim Acta 59:69–74
12. Hanai K, Ueno M, Imanishi N, Hirano A, Yamamoto O, Takeda Y (2011) Interfacial resistance of the $LiFePO_4$-C/PEO-LiTFSI composite electrode for dry-polymer lithium-ion batteries. J Power Sources 196:6756–6761
13. Yamada I, Abe T, Iriyama Y, Ogumi Z (2003) Lithium-ion transfer at $LiMn_2O_4$ thin film electrode prepared by pulsed laser deposition. Electrochem Commun 5:502–505
14. Yamada I, Iriyama Y, Abe T, Ogumi Z (2007) Lithium-ion transfer on a Li_xCoO_2 thin film electrode prepared by pulsed laser deposition – effect of orientation. J Power Sources 172:933–937
15. Baek B, Jung C (2010) Enhacement of the Li^+ ion transfer reaction at the $LiCoO_2$ interface by 1,3.5-trifluorobenzene. Electrochem Acta 55:3307–3311
16. Zhu YR, Xie Y, Zhu RS, Shu J, Jiang LJ, Qiao HB, Yi TF (2011) Kinetic study on $LiFePO_4$-positive electrode material of lithium-ion battery. Ionics 17:437–441
17. Zhong S, Wu L, Liu J (2012) Sol–gel synthesis and electrochemical properties of $9LiFePO_4{\cdot}Li_3V_2(PO_4)_3$/C composite cathode material for lithium ion batteries. Electrochem Acta 74:8–15
18. Cao J, Qu Y, Guo R (2012) $La_{0.6}Sr_{0.4}CoO_{3-1}$ modified $LiFePO_4$/C composite cathodes with improved electrochemical performances. Electrochem Acta 67:152–158
19. Zhang Y, Wang C-Y, Tang X (2011) Cycling degradation of an automotive $LiFePO_4$ lithium-ion battery. J Power Sources 196: 1513–1520
20. Ju H, Wu J, Xu Y (2013) Revisiting the electrochemical impedance behaviour of the $LiFePO_4$/C cathode. J Chem Sci 125:687–693
21. Guo ZP, Konstantinov K, Wang GX, Liu HK, Dou SX (2003) Preparation of orthorhombic $LiMnO_2$ material via the sol-gel process. J Power Sources 119-121:221–225
22. Lu D, Li W, Zuo X, Yuan Z, Huang Q (2007) Study on electrode kinetics of Li^+ insertion in $Li_xMn_2O_4$ ($0 \le x \le 1$) by electrochemical impedance spectroscopy. J Phys Chem C 111:12067–12074
23. Nobili F, Tossici R, Marassi R, Croce F, Scrosati B (2002) An AC impedance spectroscopic study of Li_xCoO_2 at different temperatures. J Phys Chem B 106:3909–3915
24. Manjunatha H, Mahesh KC, Suresh GS, Venkatesha TV (2011) The study of lithium ion de-insertion/insertion in $LiMn_2O_4$ and determination of kinetic parameters in aqueous Li_2SO_4 solution using electrochemical impedance spectroscopy. Electrochem Acta 56:1439–1446
25. Nagasubramanian G, Attia AI, Halpert G (1994) A polyacrylonitrile-based gelled electrolyte: electrochemical kinetic studies. J Appl Electrochem 24:298–302
26. Liebenow C, Luhder K (1996) Electrochemical characterization of polymer precoated electrodes. J Appl Electrochem 26:689–692
27. Munichandaiah N, Shukla AK, LScanlon LG, Marsh RA (1996) On the stability of lithium turing ageing of Li/PEO_8LiClO_4/Li cells. J Power Sources 62:201–206
28. Wang XM, Iyoda M, Nishina T, Uchida I (1997) Microelectrode investigation of the lithium redox behavior in plasticized polymer electrolytes. J Power Sources 68:487–491
29. Wang XM, Nishina T, Uchida I (1997) Application of the microelectrode technique to the kinetic study of lithium deposition/dissolution and alloying in organic solutions. J Power Sources 68: 483–486
30. Lee SI, Jung UH, Kim YS, Kim MH, Ahn DJ, Chun HS (2002) A study of electrochemical kinetics of lithium ion in organic solvents. Korean J Chem Eng 19:638–644
31. Lewandowski A, Jakobczyk P Kinetics of $Na|CF_x$ and $Li|CF_x$ systems. J Solid State Electrochem, In Press. doi:10.1007/s10008-016-3305-5
32. Xu K (2007) "Charge-transfer" process at graphite/electrolyte interface and the solvation sheath structure of Li^+ in nonaqueous electrolytes. J Electrochem Soc 154:A162–A167